Journal of
Water & Climate Change

IWA PUBLISHING

Journal of Water and Climate Change Vol 12 No 6, 2797 doi: 10.2166/wcc.2021.160

Effect of de-trending climatic parameters on temporal changes of reference evapotranspiration in the eastern Himalayan region of Sikkim, India

Vanita Pandey, Indira Taloh and P. K. Pandey*

Department of Agricultural Engineering, North Eastern Regional Institute of Science and Technology (NERIST), Nirjuli, Itanagar, Arunachal Pradesh, India
*Corresponding author. E-mail: pkpnerist@gmail.com

ABSTRACT

Reference Evapotranspiration (ET_0) is an essential factor in irrigation scheduling, climate change studies, and drought assessment. The study's main objective was to identify the influences of detrending input climatic parameters (CPs) on ET_0 using linear and nonlinear approaches throughout 1980–2015 in Gangtok, East Sikkim, India. The benchmark values of ET_0 were calculated using the global standard FAO56 Penman–Montieth equation. The ET_0-related CPs included for the analysis are maximum temperature (T_{max}), minimum temperature (T_{min}), maximum relative humidity (RH_{max}), minimum relative humidity (RH_{min}), and sunshine duration (SSH). The linear and nonlinear trends in various CPs affect ET_0 change. Linearly detrended series was obtained by linear regression method whereas, nonlinearly detrended series was obtained using the Complete Ensemble Empirical Mode Decomposition with Adaptive Noise method. Twenty-three scenarios, including the original scenario, 11 scenarios in Group 1 (CPs de-trended linearly), and 11 scenarios in Group 2 (CPs de-trended nonlinearly) were generated. Influences of T_{max} and SSH were more substantial than the influences of other CPs for both Group 1 and Group 2. The SSH masked the weak influence of other CPs. The effects of the trends in CPs, especially of SSH and T_{max}, were clearly shown. The ET_0 values decreased significantly during 1980–2015; however, no significant decreasing trend was observed in the case of SSH, during the same period. The nonlinear detrending gave closer results to the benchmark values as compared to linear detrending because of non-monotone variations of the ET_0 and CPs. Therefore, the results from nonlinear detrending were more plausible as compared to linear detrending. The diminishing trend of ET_0 prompted an overall alleviation of the dry spell, hence there would be a somewhat lower risk of water use in the study region.

Key words: CEEMDAN, climatic parameters (CPs), linear and nonlinear detrending, reference evapotranspiration (ET_0)

HIGHLIGHTS

- Sunshine hour (SSH) and maximum temperature (T_{max}) independently were the most important variables affecting reference evapotranspiration (ET_0).
- Detrending of minimum temperature and relative humidity insignificantly affects the ET_0 process.
- Effect of detrending sunshine hour (SSH) masked the increasing trend effects of other climatic parameters on ET_0.
- ET_0 estimated by nonlinear detrending of climatic parameters (CPs) was satisfactory and convincing compared to linear detrending.

INTRODUCTION

Climate-related risks to food security, agriculture, livelihoods, and water supply are anticipated to increment with global warming of 1.5 °C above temperatures in the pre-industrial period and increment further with 2 °C by 2100 (Intergovernmental Panel on Climate Change (IPCC 2019)). In the context of global warming and climate change, accurate estimation and prediction of evapotranspiration is of vital importance in the studies related to hydrological modeling, climate change prediction, water resources planning and management, irrigation scheduling, and determining crop water requirement. The reference evapotranspiration (ET_0) can be used as an index to assess agricultural water demand. The FAO had identified the FAO56 Penman–Montieth (FAO-56-P-M) model as a benchmark for the precise estimation of ET_0 following an extensive comparison with lysimetric measured data globally (Allen *et al.* 1998).

A literature survey confirms that studies worldwide reported that the trend of ET_0 was found to have increased or decreased in various areas of the world. Studies reported both increasing and decreasing trends in Iran (Dinpashoh *et al.* 2011), China (Mo *et al.* 2017; Liu *et al.* 2020), and India (Sonali & Nagesh Kumar 2016). Significant increasing trends of ET_0 were reported in the Korean Peninsula (Ghafouri-Azar *et al.* 2018), in Iran (Azizzadeh & Javan 2015), in central Europe (Zaninović &

Gajić-Čapka 2000), and China (Niu *et al.* 2019). The strong decreasing trend in ET_0 was observed in Canada (Burn & Hesch 2007), in the United States (Golubev *et al.* 2001), in Australia (Donohue *et al.* 2010), in India (Verma *et al.* 2008; Jhajharia *et al.* 2012; Yadav *et al.* 2016; Goroshi *et al.* 2017), and in China (Niu *et al.* 2019).

The reference evapotranspiration is a multivariate parameter and function of climatic parameters (CPs), namely temperature (T), relative humidity (RH), solar radiation (Rs), and wind Speed (Ws). The temporal variability of CPs is mainly responsible for the upward and downward trend in ET_0 (Li *et al.* 2017).

The analysis of impacts of CPs on ET_0 is useful to know the climatic change impacts on ET_0 (Xu *et al.* 2006; McVicar *et al.* 2012). There are two conventional approaches to quantify the influence of CPs on ET_0. The first approach is based on sensitivity analysis (Mckenney & Rosenberg 1993; Tabari & Hosseinzadeh Talaee 2014; Zhao *et al.* 2014; Patle & Singh 2015), while the second method re-calculates ET_0 by using detrended CPs (Huo *et al.* 2013; Zhao *et al.* 2014; Li *et al.* 2017). However, these studies analyzed only the impacts of the single climatic parameter on ET_0, not the simultaneous effects of different factors on ET_0. Since CPs change simultaneously, a single CP such as a different temperature (maximum T(max) and minimum T(min)) may vary in a different pattern. It is not sufficient to know only the influences of a single CP on ET_0. Studies mentioned above have not recognized the influence of different temperature factors (T_{min} and T_{max}) on ET_0. Additionally, eliminating linear trends from CPs is sufficient, yet eliminating the nonlinear trend in CPs is vital because most CPs change nonlinearly with time.

Statistical trend analysis can be further carried out under parametric and nonparametric analysis. The difference between the two is the way of using collected data. In the parametric analysis, actual parameters are used to determine the trend, considering data are normally distributed and independent. However, the nonparametric test does not necessarily require data to be normally distributed. The most often utilized nonparametric test for identifying the pattern in data is the Mann–Kendall test (Kahya & Kalayci 2004; Jayawardene *et al.* 2005; Burn & Hesch 2007; Li *et al.* 2007; Theppraisit *et al.* 2009; Aksu *et al.* 2010; Espadafor *et al.* 2011; Tabari & Marofi 2011; Jhajharia *et al.* 2012; Karmeshu 2012; Kousari & Ahani 2012; Shadmani *et al.* 2012; Gocic & Trajkovic 2014) to detect the trend in climatic time series.

Before implementing any parametric or nonparametric tests, the data's independence should be checked using the lag-1 autocorrelation test. The trend-free pre-whitening with Mann–Kendall is one common approach, which shows the relation between a linear trend and a lag-one autocorrelation (Yue *et al.* 2002, 2003; Dinpashoh *et al.* 2011). The elimination of trend components before pre-whitening removes the serial correlation from the time series. The elimination of positive serial correlation components through pre-whitening causes the magnitude of the prevailing trend to reduce. In their variance correction approach, Hameed & Rao (1998) reported that the existence of positive or negative serial correlation results in an increase or decrease in the variance of Mann–Kendall test statistic (S). Therefore, to prevent the effect of the problem, the variance correction approach was recommended.

Detrending is a mathematical or statistical operation of removing trends from a climatic time series. The detrending technique is a combined methodology that considers both the sensitivity coefficient and the rate of climatic factors. The empirical mode decomposition (EMD) is a versatile technique developed to examine non-stationary and nonlinear signals. It comprises a nearby and completely information-driven detachment of a signal in rapid and moderate oscillations. The decomposition is produced from the traditional assumption that any data consist of oscillation's various basic intrinsic modes.

Every mode might be linear and may have a similar number of extrema and zero intersections. However, EMD encounters a few issues, such as oscillation of unique amplitude in a mode of the existence of fundamentally the same oscillations in various modes, called 'mode mixing.' Torres *et al.* (2011) suggested an ensemble empirical mode decomposition (EEMD) with the addition to Gaussian white noise over EMD. The addition of Gaussian white noise eliminates the problem of mode mixing (Guo *et al.* 2016). Sang *et al.* (2014) in a comparison of the Mann–Kendall and EMD method of trend analysis reported that EMD can be an effective alternative for trend identification of hydrological time series. Even though EEMD by then was proven to help investigate geophysical data, it additionally has a few disadvantages. The main disadvantage is that the signal reproduced by EEMD has a residual noise, and the problem of mode mixing still exists in outermost applications to real data. Antico *et al.* (2014) developed the CEEMDAN (complete ensemble empirical mode decomposition with adaptive noise) method. The CEEMDAN gives an accurate reconstruction of the original signal and an apparent spectral detachment of modes, thus eliminating the mode mixing problem (Antico *et al.* 2014; Marusiak & Pekar 2014). Antico *et al.* (2014) successfully applied CEEMDAN on river discharge data to determine the time-scale components of hydrological time series and concluded that it is the powerful method for extracting physically meaningful information from hydroclimatic data. Therefore,

CEEMDAN is a powerful means for separating physically relevant data from hydroclimatic time series, particularly when the previously mentioned issues are experienced.

The authors did not find the same or at least similar earlier conducted studies which analyzed the influence of removing both (linear and nonlinear) trends from various CPs on ET_0 in India. In this case study, we performed a trend analysis of different CPs. In the next step, CPs are detrended both linearly and nonlinearly to study the effect of detrending the CPs on temporal variations of annual reference evapotranspiration (ET_0) Gangtok, Sikkim.

METHODS

Description of the study area and data sets

The study area is situated in the eastern Himalayas, according to the agro-climate zone of India (Government of India 1989). The investigation was conducted in east Sikkim, which has a latitude range between 27°9′ and 27°25′ N and longitude from 88°27′ and 88°56′ E, and covers about 900 km^2 area. Geographically, East Sikkim occupies the southeast corner of the state (Figure 1). Almost the entire east Sikkim is hilly, with an elevation range of 811–1,650 m. The average annual sum of the precipitation during the observed period at Gangtok is about 3,090 mm. The average annual temperatures (T_{max} and T_{min}) during the observed period were 22.97 and 13.72 °C, respectively (Table 1). The district's average index of wetness is more than one, and the number of rainy days ranges from 128 to 205 days. The study region gets a significant part of precipitation from the south-west monsoon. For most periods in the course of a year, the climate is cold and humid as precipitation occurs each month. Pre-monsoon rain occurs in April–May, and monsoon (south-west) operates normally from May and continues up to early October. The descriptive statistics of ET_0 and different meteorological parameters are depicted in Table 1.

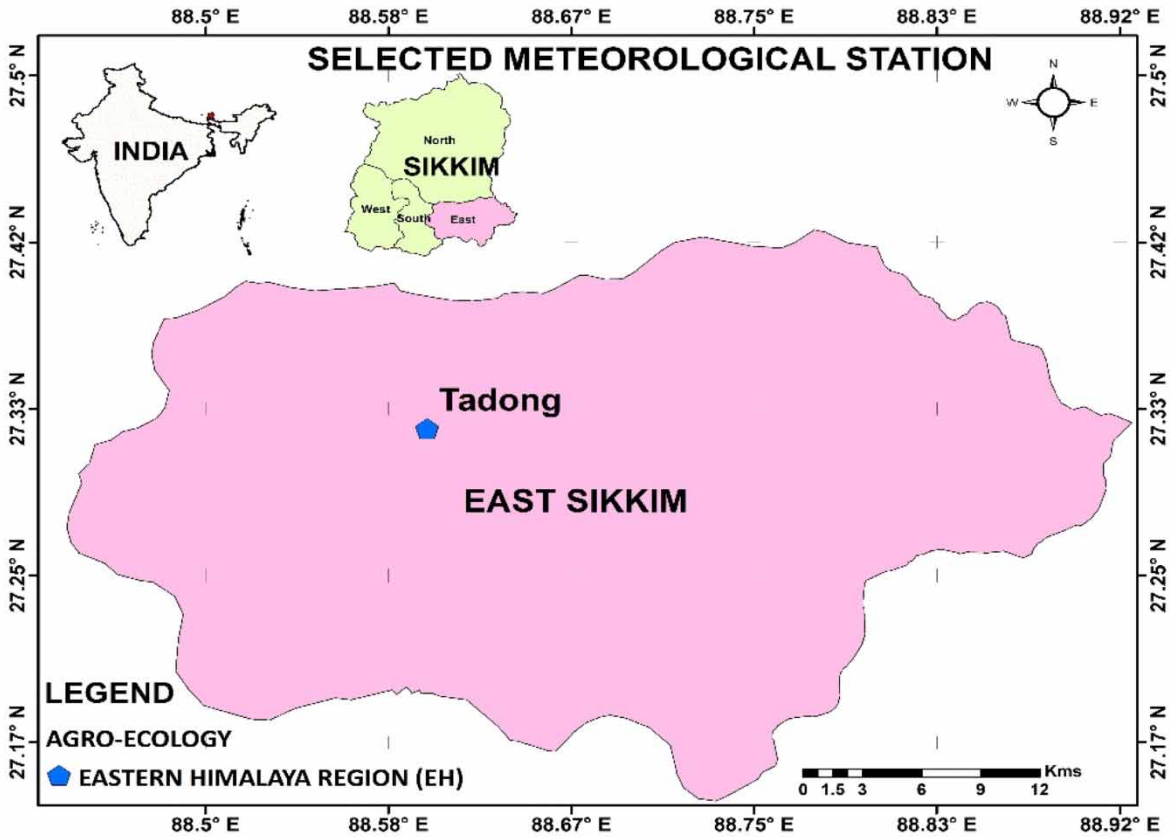

Figure 1 | Location map of the study area.

Table 1 | Descriptive statistic of reference evapotranspiration and different meteorological parameters during (1980–2015) at Gangtok Sikkim

Time scale	Statistics	T_{max}	T_{min}	RH_{max}	RH_{min}	SSH	ET_0
Annual	Average	22.97	13.72	86.28	55.72	3.76	2.85
	Max	33.50	20.60	94.60	83.50	9.90	5.51
	Min	11.80	3.30	67.60	24.90	0.00	1.53
	Std	3.97	4.70	4.61	11.40	1.48	0.66
	CV	0.17	0.34	0.05	0.20	0.39	0.23
Monsoon	Average	26.40	18.84	90.14	68.54	2.59	3.20
	Max	33.45	20.60	94.20	83.50	5.60	5.65
	Min	21.70	14.40	75.50	51.70	1.00	2.62
	Std	1.47	1.36	2.42	5.60	0.89	0.55
	CV	0.06	0.07	0.03	0.08	0.34	0.17
Post monsoon	Average	19.56	9.64	84.37	48.86	4.13	2.24
	Max	26.70	17.20	94.40	69.00	7.90	3.28
	Min	11.80	3.30	71.70	24.90	1.00	1.55
	Std	3.51	3.25	3.71	7.35	1.46	0.38
	CV	0.18	0.34	0.04	0.15	0.35	0.17
Pre monsoon	Average	24.09	13.68	84.30	50.12	4.64	3.50
	Max	28.10	18.30	94.60	68.30	7.30	5.39
	Min	17.20	6.70	67.60	29.60	2.10	2.82
	Std	2.33	2.56	4.90	7.77	0.95	0.42
	CV	0.10	0.19	0.06	0.15	0.21	0.12

Note: T_{max}: maximum temperature, °C; T_{min}: minimum temperature, °C; RH_{max}: maximum relative humidity, %; RH_{min}: minimum relative humidity, % ; SSH: sunshine duration, (hours); ET_0: reference evapotranspiration, mm d^{-1}.

Modeling of reference evapotranspiration (ET_0)

The FAO 56 Penman–Monteith (FAO56-P-M) (Allen *et al.* 1998) equation is used as the standard method for the computation of ET_0 from meteorological data. The mathematical equation of the FAO56-P-M, ET_0 can be written as:

$$ET_0 = \frac{0.408\Delta(R_{net} - G_{hf}) + \gamma\frac{900}{\overline{T}+273}W_2(e_s - e_a)}{\Delta + \gamma(1 + 0.34W_2)} \quad (1)$$

where ET_0 is reference evapotranspiration (mm d^{-1}), R_{net} is net radiation (MJ m^{-2} d^{-1}), $(e_S - e_a)$ is difference between the saturation vapor pressure e_S (kPa) and the actual vapor pressure e_a (kPa), Δ is the slope of the saturation vapor pressure–temperature curve (kPa °C^{-1}), γ is the psychometric constant (kPa °C^{-1}), W_2 is the wind speed at 2 m height (m s^{-1}), $\overline{T}$ is the average air temperature (°C), and G_{hf} is the monthly soil heat flux density (M J m^{-2} d^{-1}). The detailed procedure for estimating different secondary parameters of FAO-56-P-M can be found elsewhere (Allen *et al.* 1998).

Data management for analysis

The daily meteorological data from 1980 to 2015 for various CPs namely T_{max} (°C), T_{min} (°C), RH_{max} (%), RH_{min} (%) and SSH (h) to apply FAO56-P-M were collected from the Indian Meteorological Department, Tadong, Sikkim. The mean monthly and seasonal ET_0 was estimated using the FAO56-P-M equation. The baseline values were fixed as mean values of monthly, seasonal ET_0, and CPs.

Trend and change point (T_{AC}) analysis

The CPs, namely T_{max} (°C), T_{min} (°C), RH_{max} (%), RH_{min} (%), SSH (h), and ET_0 (mm d^{-1}), were used for trend and abrupt change year (T_{AC}). The modified nonparametric Mann–Kendall (MM-K) (Yue & Wang 2004) was used for trend analysis. The MM-K statistics (Z_c) can be estimated using the Mann–Kendall method (Mann 1945; Kendall 1975) by eliminating the influence of serial autocorrelation in x_i ($i = 1, 2, 3 \ldots n$, where n is the total number of years). The correction in MM-

K statistics Z's variance was performed, as in Hameed & Rao (1998) and Sonali & Nagesh Kumar (2013).

$$\mathrm{Var}^*(Z) = \mathrm{V}(Z)\frac{n}{n^*} \tag{2}$$

where n is the number of data points, n^* is the effective sample size, and n/n^* is the correction factor for serial correlation in sample data, $V(Z)$ is the variance of Z of MK (Mann–Kendall) statistic for the time series, estimated using the following relationship:

$$V(Z) = \frac{n \times (n-1) \times (2n+5)}{18} \tag{3}$$

The existence of tied ranks (equal observations) in the data results in a reduction of the variance of Z to become,

$$V(Z) = \frac{n \times (n-1) \times (2n+5)}{18} - \sum_{i=1}^{k} \frac{T_i \times (T_i-1) \times (2T_i+5)}{18} \tag{4}$$

where k is the number of groups of tied ranks, each with T_j tied observations.

The correction factor n/n^* in Equation (2) can be estimated as:

$$\frac{n}{n^*} = 1 + \frac{2}{n(n-1)(n-2)} \sum_{i=1}^{n-1} (n-l)(n-l-1)(n-l-2) r_l^R \tag{5}$$

where r_l^R is the lag-l serial correlation coefficient of rank $R_{X\mathrm{t}}$ of the sample data X_t. Salas *et al.*'s (1980) equation given below is used for estimating values r_k^R by substituting the sample data X_t by their ranks $R_{X\mathrm{t}}$.

$$r_l = \frac{\frac{1}{n-l}\sum_{s=1}^{n-l}[X_s - E(X_s)][X_{s+l} - E(X_s)]}{\frac{1}{n}\sum_{s=1}^{n}[X_s - E(X_s)]^2} \tag{6}$$

$$E(X_s) = \frac{1}{n}\sum_{s=1}^{n} X_s \tag{7}$$

where r_l is the serial correlation coefficient at lag1 of the sample (X_s), and $E\ (X_s)$ is the mean of the sample.

The modified standardized MK statistic Z_c can be estimated as:

$$Z_\mathrm{c} = \begin{cases} \dfrac{Z-1}{\sqrt{\mathrm{Var}^*(Z)}} & Z > 0 \\ 0, & Z = 0 \\ \dfrac{Z+1}{\sqrt{\mathrm{Var}^*(Z)}} & Z < 0 \end{cases} \tag{8}$$

In the above relation, the value of Z can be estimated as (Kahya & Kalayci 2004):

$$Z = \sum_{k=1}^{n-1}\sum_{j=k+1}^{n} \mathrm{sign}(x_j - x_k) = \begin{cases} +1 & \text{if } (x_j - x_k) > 0 \\ 0 & \text{if } (x_j - x_k) = 0 \\ -1 & \text{if } (x_j - x_k) < 0 \end{cases} \tag{9}$$

The increasing or decreasing trend in x_i is identified based on Z_c's calculated values at a 5% significance level (greater than 0 and $-1.96 \geq Z_c \geq 1.96$) on r_1 (lag-l autocorrelation). The magnitude of the trend was identified using Sen's (Sen 1968) method (Adarsh & Janga Reddy 2015).

The change point of the trend was analyzed using the sequential Mann–Kendall (SQM-K) test (Liu *et al.* 2008; Sonali & Nagesh Kumar 2013; Sayemuzzaman & Jha 2014; Jones *et al.* 2015). The SQM-K is a sequential progressive S_q (t) and backward S_q' (t) analysis of the MK test. In this case, sequential progressive S_q (t) and backward S_q' (t) series intersect or diverge from each other for an extended period. The beginning of the year of divergence exhibits the T_{AC}. In S_q (t) analysis, the number of cases X_j $(j = 1,2,3 \ldots n) > X_k$ $(k = 1, 2 \ldots j-1)$, denoted by $n_{t,}$ is counted at each comparison. In S_q (t) estimation, the number of times, N_t for which $X_j > X_k$ was counted. The sequential test statistics S_t are calculated by:

$$S_t = \sum_{i}^{n} N_t \tag{10}$$

The mean and variance of the test statistics are calculated as follows:

$$E(S) = \frac{n(n-1)}{4} \tag{11}$$

$$\mathrm{Var}(S_t) = \frac{j(j-1)(2j+5)}{72} \tag{12}$$

The S_q (t) is estimated as:

$$S_q(t) = \frac{S_t - E(S)}{\sqrt{\mathrm{Var}(S_t)}} \tag{13}$$

The S_q' (t) was determined, estimated similarly, with x_i's termination point being the beginning.

Detrending of CPs

The linear detrended data series is obtained by eliminating the original data series linear trend each year. The original data series value is added to the detrended data series to maintain a close variation range to the original data.

In the present study, the nonlinear detrending of the various CPs was performed using the CEEMDAN technique (Antico *et al.* 2014). The CEEMDAN technique of signal processing decomposes the input data to intrinsic mode functions (IMFs) with varying phase and amplitude and residuals (trend). An IMF is a continuous map, which fulfills the following condition (Huang *et al.* 1998): (a) the number of zero intersections and the extrema must be equivalent or have a difference limited to one, (b) the mean estimation of the upper envelope framed by local maxima and lower envelope shaped by lower minima must be equivalent to zero at any point. Within this condition of IMF, the decomposition procedure of CEEMDAN is given below:

1. Show the input signal, $x(t)$.
2. Identify the local maxima and minima of time series.
3. Calculate both upper and lower envelopes by joining all local maxima using any suitable signal decomposition method, such as cubic splines.
4. Calculate the local average value (m_1) between both upper and lower envelopes.
5. The first component is calculated as $h_1(t) = x(t) - m_1(t)$.

If the first component (as computed in step 5) does not fulfill the IMF's conditions, repeat step 2 to step 5 by considering h_1 (t) as the next input signal. This procedure is repeated for k times until it fulfills the IMF conditions i.e., h_{1k} $(t) = h_{(1\text{-}k)}$ $(t) - m_{1k}(t)$, then c_1 $(t) = h_{1k}$ (t) is considered as the first IMF. Then residue r_1 is determined by subtracting the first IMF from x (t) (i.e., $r_1(t) = x$ $(t) - c_1(t)$). Continue this procedure for r_1 until series r_l(t) becomes a monotonic function such that the

extraction of further IMF is not possible. Therefore, signal $x\ (t)$ can be illustrated as:

$$x(t) = \sum_{i=1}^{l=1} c_i(t) + r_l(t) \tag{14}$$

The CEEMDAN method works by adding different realization of white noise to an original time series to obtain a series $x_i\ (t) = x\ (t) + w_i\ (t)$, where $w_i\ (t)$ are the white realization and then decomposing it via the EMD method. Procured from the first series $x_i\ (t)$, one can compute the first series component $x\ (t)$ as

$$c^{\sim 1}(t) = 1/I \sum_{i=1}^{I} c_i^{(1)}(t) \tag{15}$$

The first residue is computed as:

$$r^1(t) = x(t) - c^{\sim 1}(t) \tag{16}$$

Moreover, then, $c^{-1}\ (t)$ is calculated as the average of the individual series of the implementation of $r^1\ (t)$ series along with the first component of EMD white noise decomposition $w_i\ (t)$.

The CEEMDAN was preferred for obtaining the nonlinearly detrended data series using the 'Rlibeemd' package (Luukko *et al.* 2016) of R software in the present study. The original data of various CPs (T_{max}, T_{min}, RH_{max}, RH_{min}, SSH) are imported into the software. With the help of the Rlibeemd package, CEEMDAN decomposes the input data to IMFs and a residual series.

Scenarios of ET_0 estimated using the detrended CPs

In the present study, the main objective is to compare the effects of linear and nonlinear detrending (i) between different temperature factors (T_{max}, T_m, T_{min}) and (ii) non-temperature factors (i.e., RH_{max}, RH_{min}, and SSH) on changing ET_0. The number of total combinations created was 23, including the original scenario CP1. The original scenario CP1 is estimated from the observed CPs, and two other groups (i.e., linear and nonlinear) are created. Both the scenarios contain 11 different combinations of recalculated ET_0 using various sets, as shown in Table 2 of the observed and detrended CPs.

Single or multi CPs were detrended from Group 1, consisting of a linear trend, and Group 2 of nonlinear trends. The detrended CPs with other observed CPs were utilized for the re-estimation of ET_0. A total of 23 combinations of ET_0, including the original set CP1, CP2 to CP11 in Group 1, and CP2 to CP11 in Group 2, are applied. In the combination CP2 to CP4, the influences of detrending one or more temperature factors are contrasted gradually, i.e., in CP2, T_{max} is detrended, CP3 T_{min} is detrended, CP4 both T_{max} and T_{min} are detrended. At the same time, in CP5 to CP11, the influences of detrending one or more non-temperature factors CP5 to CP10 are non-temperature factors, i.e., in CP5 RH_{max} is detrended, CP6 RH_{min} is detrended, CP7 both RH_{max} and RH_{min} are detrended, CP8 SSH is detrended, CP9 SSH and RH_{max} are detrended, CP10 SSH and RH_{min} are detrended, in CP11 SSH, RH_{max} and RH_{min} are detrended. In CP12, all the observed CPs are detrended. The effect level between temperature and non-temperature parameters could be shown by comparing scenarios (CP2 to CP4) with scenarios (CP5 to CP11) (Table 2).

Table 2 | Combinations de-trended CPs in the predefined 12 scenarios

	Scenarios/ Combinations											
Climatic parameters	**CP1**	**CP2**	**CP3**	**CP4**	**CP5**	**CP6**	**CP7**	**CP8**	**CP9**	**CP10**	**CP11**	**CP12**
T_{max} (°C)		*		*								*
T_{min} (°C)			*	*								*
RH_{max} (%)					*		*		*		*	*
RH_{min} (%)						*	*			*	*	*
SSH (h)								*	*	*	*	*

*Climatic parameter de-trended in the scenario and used for re-estimating ET_0.

RESULTS

Trend analysis and comparison between Sen's slope (*b*) and regression slope

In the Mann–Kendall test, parameters like modified Mann–Kendall Statistics (Z_c) and Sen's slope (b) were assigned to distinguish the increasing or decreasing trends in the climatic time series parameters. From Table 3, it is clear that at a 5% level of significance, the estimated Z_c value predicts a significant increasing trend for T_{min}. In contrast, a significant decreasing trend was observed for sunshine duration and evapotranspiration. The remaining CPs show an insignificant increasing trend at a 5% level of significance (Table 3).

The results obtained for abrupt change year (T_{AC}) are also presented in Table 3. The T_{AC} for $T_{max,}$ RH_{max}, and RH_{min} was observed in 1985, 1983 and 1982, respectively. However, for $T_{min,}$ SSH, and ET_0, T_{AC} was not observed as the two series, S_q (t) and S_q' (t) did not cross each other. The Sen's slope b for ET_0 and 5 CPs vary to a small degree. The magnitude of positive Sen's slope follows a sequence of $T_{min} > RH_{min} > RH_{max} > T_{max}$ that the mean rate of increase of T_{min} per year is maximum for the studied parameters. In contrast, the rate of increase of T_{max} is the lowest of the studied parameters. However, for sunshine duration and evapotranspiration, the value of the Sen slope (b) is negative. Total sunshine duration decreases at a rate of 0.049 h per year, and evapotranspiration decreases at a rate of 0.078 mm d^{-1} per year. This helps to determine the most critical parameter responsible for negative trends in ET_0. The same table also depicts that the magnitude of Sen slope (b) and the regression slope (RS) of related CPs are close. Although Sen slope (b) detector is nonparametric and the RS technique is a parametric technique, both the techniques are linear. Therefore, a minor difference in the b and RS values gives very similar results for analyzing the detrending impacts on reference evapotranspiration and verified the correctness of using RS values for detrending.

Temporal changes of CPs and ET_0 and their trends

Temporal changes in annual CPs and their linear trends and nonlinear trends during the study period 1980–2015 are shown in Figure 2(a)–(f). Figure 2(a) shows that the linear and nonlinear trend lines are separate until the nonlinear line decreases and meets the linear range. The linear trend line of T_{max} is similar to the nonlinear trend from 1996 onwards until 2015. Before 1996, nonlinear trends are on a higher side than the linear trend. The significant increasing linear trend of T_{min} (Figure 2(b)) is different from the significant increasing nonlinear trends except in 1986–1988 and 2006–2008. The fluctuation patterns of RH_{max} (Figure 2(c)) and RH_{min} (Figure 2(d)) were generally similar. However, the magnitude of fluctuation in RH_{min} was more than the RH_{max}. In RH_{max} and RH_{min} trends, there was a weak increase from 1980–2015. For RH_{max}, both linear and nonlinear trends differed insignificantly (the linear trend is minuet differing from the nonlinear trend) except in 1986–1991 and 2010–2012. For RH_{min}, the linear trend was generally different from the nonlinear trend except in 1987 and 2001, where the nonlinear trend increased and decreased back, respectively. For the SSH (Figure 2(e)), both the linear and nonlinear trends sharply decreased from 1980–2015. The linear trend was generally different from nonlinear trends throughout the study period except in 1988 and 2004–2005. From the nonlinear trends, SSH seems to decrease, and the nonlinear variation of SSH adds to the nonlinear change of ET_0. These major or minor differences in linear and nonlinear trends in basic input parameters for ET_0 estimation create a difference in recalculated ET_0 after linear and nonlinear detrending.

Table 3 | Trend and abrupt change year analysis of CPs

CPs	Z_c	*b*	Regression slope	T_{AC}
T_{max} (°C)	1.24	0.006 (°C per year)	0.0044 (°C per year)	1985
T_{min} (°C)	3.93**	0.095 (°C per year)	0.0978 (°C per year)	–
RH_{max} (%)	0.34	0.031 (% per year)	0.0214 (% per year)	1983
RH_{min} (%)	0.4	0.013 (% per year)	0.021 (% per year)	1982
SSH (h)	−5.65**	−0.049 (h per year)	−0.052 (h per year)	–
ET_0 (mm d^{-1})	−4.57**	−0.0078 (mm d^{-1} per year)	−0.0078 (mm d^{-1} per year)	–

Z_C, MMK statistic; *b*, Sen's slope; T_{AC}, abrupt change year, **significant trend at 5% significance level.

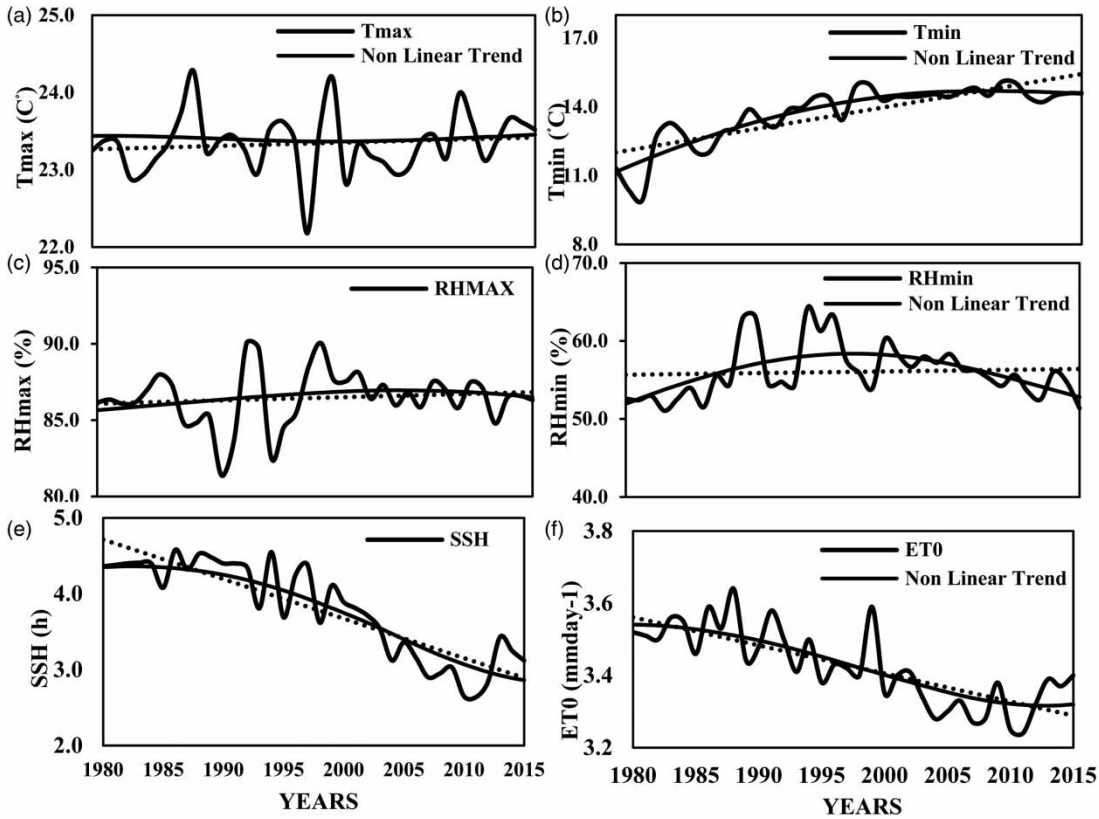

Figure 2 | Temporal variations of annual CPs, annual ET_0, and their linear and nonlinear trends during 1980–2015. The graphics (a)–(f) corresponding to the respective CPs.

The distinct variations of the five principal CPs resulted in a difference of ET_0. The ET_0 variation (Figure 2(f)) and its linear and nonlinear trend represented a decreased trend. The significant difference between the linear and nonlinear trends in ET_0 contributes to the difference in regenerated ET_0 between Group 1 and 2.

Impact of removing linear trends from annual CPs on ET_0

In this analysis, the ET_0 was recalculated using the linearly detrended CPs (Table 2) from Group 1 (linearly detrended) throughout the study period, i.e., from 1980 to 2015, and compared the recalculated ET_0 with the original calculated ET_0 under Scenario 1 (CP1).

For CP2, as depicted in Figure 3(a), the recalculated ET_0 values obtained after detrending the T_{max} are lower throughout the study years except in 1997, where the recalculated value is higher than the CP1 value. The results of the study showed that although the T_{max} is insignificantly increasing during the study period, the ET_0 value decreased. For CP3, the recalculated ET_0 values obtained after detrending the T_{min} are higher during 1980–1983, 1986–1988; from 1993 to 2010, the detrended ET_0 is slightly lower than the CP1 ET_0 (Figure 3(b)), and from 2011 to 2015, the detrended ET_0 is the same as CP1 ET_0. However, T_{min} is significantly increased during the study period but detrending of T_{min} did not affect the ET_0 values. Comparing CP4 and CP1 (Figure 3(c)) shows the decreasing values of ET_0. The recalculated ET_0 values are higher during 1981–1982 and in 1997. Overall, the detrended ET_0 is lower than the CP1 ET_0.

The findings of the study showed that although T_{max} and T_{min} have been increased during the study period, however, detrending both T_{max} and T_{min} resulted in a decrease in the ET_0 value. Thus, it may be concluded that detrending of T_{max} and T_{min} has a negative effect on ET_0. Thus, for temperature parameters, except for scenario CP3 (T_{min} de-trended), the recalculated ET_0 was below the ET_0 curve of CP1, which concludes that detrending T factors (CP2, CP3, CP4) result in decreasing ET_0.

Detrending RH parameters (CP5 to CP7), as depicted in (Figure 3(d)–(f)), showed a slight increase in ET_0 in all three cases. Hence, an insignificant increase in both RH_{max} and RH_{min} did not affect the decreasing trend of ET_0. Overall, the significant decreasing trend of sunshine duration (CP8) explains the decreasing trend of evapotranspiration (Figure 3(g)). After 2002, the

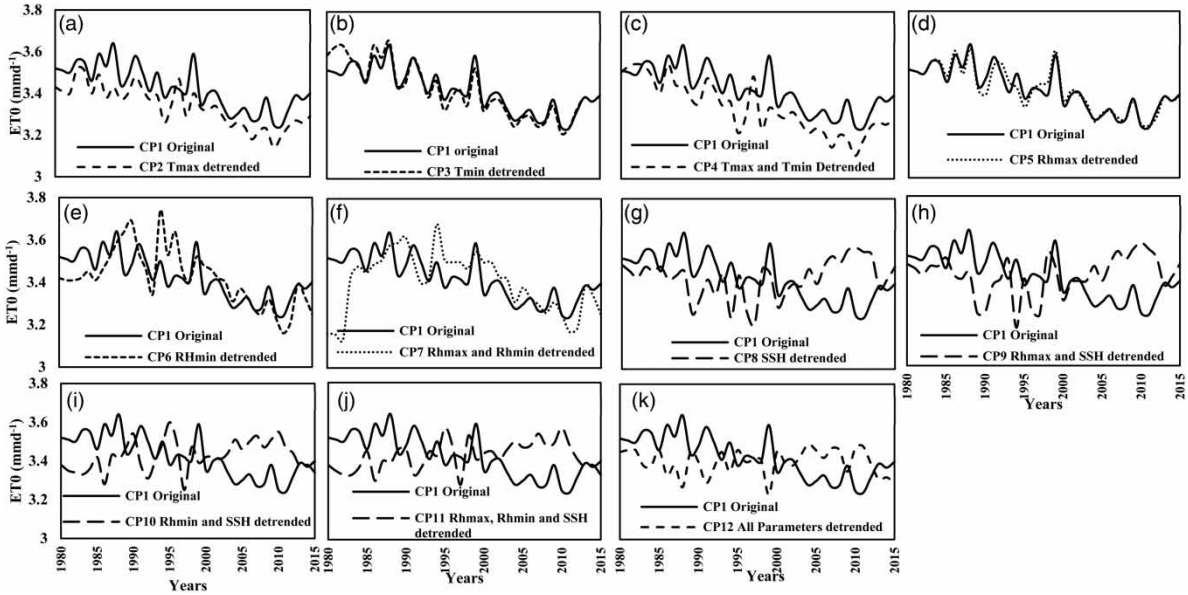

Figure 3 | Variations of annual original ET_0 (CP1) and linearly de-trended CPs (a–k) ET_0 over 1980–2015.

recalculated ET_0 is higher than that estimated in scenario CP1. Detrending of sunshine duration counters the detrending effect of humidity factors CP9, CP10, and CP11, or we can conclude that the effect of the significantly decreasing sunshine duration decreasing ET_0 values is much stronger than an insignificant increase in RH factors (Figure 3(h)–(j)).

Variation in ET_0 for CP1 and CP12 (detrending all the CPs) is similar to that obtained by detrending sunshine duration and RH (CP11) (Figure 3(k)). The result shows that with the decreasing trend in sunshine duration the decreasing trend in ET_0 is much stronger than an insignificant increase in T_{max} and a significant increase in T_{min}.

Impact of removing nonlinear trends from annual CPs on ET_0

For nonlinear detrending, CP2 insignificantly affects the variation in ET_0 during the study period (Figure 4(a)). Analysis of Figure 4(a) revealed that the original ET_0 and the values of recalculated ET_0 of CP3 show decreasing values of ET_0 for

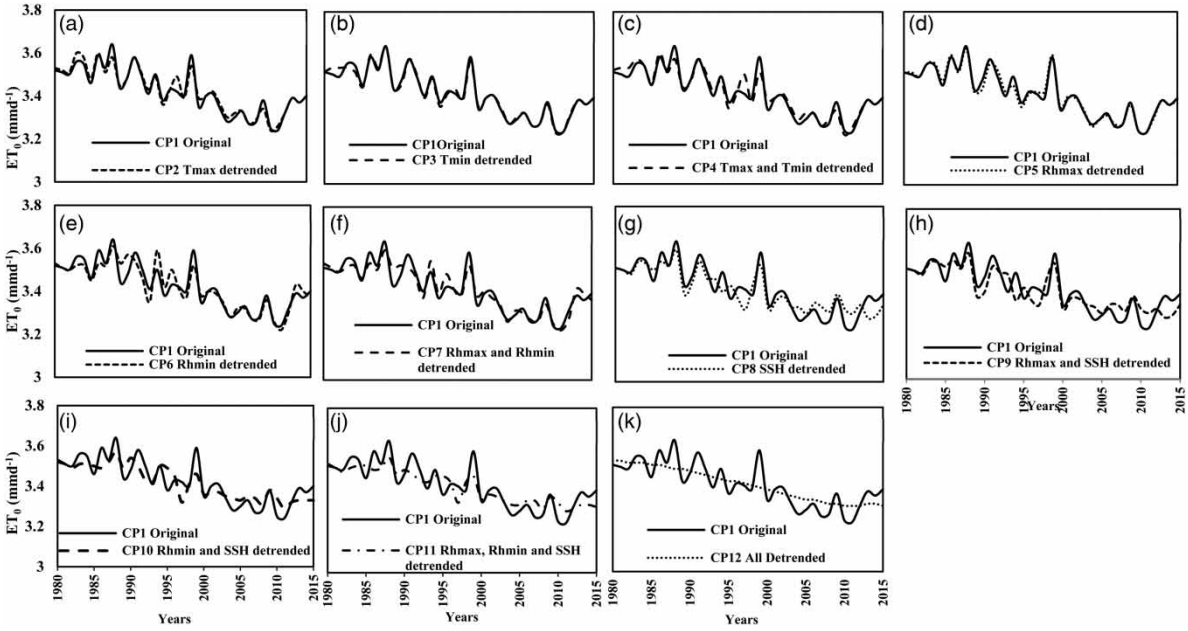

Figure 4 | Variations of annual original ET_0 (CP1) and nonlinearly de-trended CPs (a–k) ET_0 over 1980–2015.

both the scenarios. The estimates of recalculated ET_0 for CP3 (Figure 4(b)) are the same as the CP1 from 1985 onwards except for 1981–1982 and 1983. The results show that although the T_{min} is significantly increased during the study period, detrending the T_{min} did not affect ET_0. A similar insignificant impact was observed for CP4 (Figure 4(c)). The detrending of both the T_{max} and T_{min} has a negligible effect on ET_0. The increasing trend of RH_{max} and RH_{min} has an insignificant effect on ET_0 after nonlinear detrending CP5, CP6, and CP7 (Figure 4(d)–(f)). The findings of the study revealed that the detrending of RH_{max} and RH_{min} has an insignificant effect on ET_0. However, the impact of decreasing sunshine duration CP8 (Figure 4(g)) on reducing ET_0 is much more substantial than an insignificant increase in RH factors, which is similar to linear detrending. The ET_0 curve of CP12 (Figure 4(k)) increased as CP8, CP9, and CP10 (Figure 4(g)–(i)) when compared with CP1. Thus, in the annual series, for both the linear and nonlinear detrending, sunshine duration is the dominant climatic parameter to explain the decreasing trend of ET_0 in the region. Hence, we can conclude that the detrending sunshine hour surpasses the detrending of other selected CPs.

Impact of detrending all the CPs on ET_0

The original ET_0 (CP1) was compared with scenario CP12 of both Group 1 and Group 2 to know the effect of detrending if all the CPs were detrended. Thus obtained, the results are presented in Table 4 and Figure 5 (for both Group 1 and Group 2). From Table 4, it is clear that the trend and intercept obtained by linear regression were similar for both original ET_0 and non-linearly detrended ET_0 for scenario CP12, whereas, trend and intercept for linearly detrended ET_0 was not identical to the other two scenarios. However, the nature of the trend was decreasing in all the scenarios (Figure 5). Findings support that the linear detrending of CPs significantly influences ET_0 compared to nonlinear detrending. However, the results obtained by nonlinear detrending are more convincing than linear detrending based on the analysis of trend and intercept (Table 4).

Except for scenario CP12, there is no other scenario that combines the temperature and non-temperature factors because the results from the present study show that (i) the impact of detrending two temperature factors on declining ET_0 is most significant when compared with the effect of detrending single temperature factors. Furthermore, the effect of detrending T_{max} and SSH as a single parameter was more significant than detrending RH factors and T_{min}, which accentuate the critical roles of T_{max} and SSH on the varying ET_0 as an individual factor.

Therefore, it is not required to add more scenarios to illustrate the impacts of the detrending of combined RH_{max}, RH_{min}, and T_{min} because their impacts will be small. Therefore, CP12, which contains CPs of temperature and non-temperature factors, would thoroughly illustrate the effects of detrending CPs on ET_0.

Table 4 | Comparison among CP1, and de-trended CP12 (linear and nonlinear)

S No	Scenarios	Slope of linear regression trend line	Intercept of linear regression
1	CP1 (original ET_0)	−0.0078	18.989
2	CP12 (linear de-trended)	−0.0003	4.018
3	CP12 (nonlinear de-trended)	−0.0074	18.213

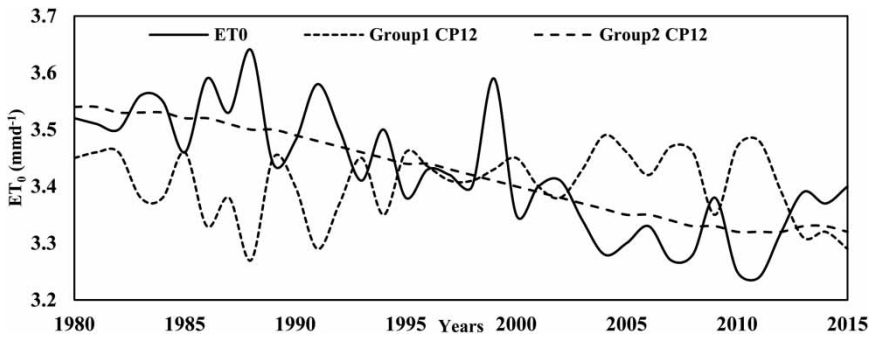

Figure 5 | Variation of annual ET_0 for CP1, CP12 for the Group 1 and CP 12 for Group 2 over 1980 to 2015.

ΔET_0 variations under different scenarios

ΔET_0 is the difference in the original ET_0 and the recalculated ET_0 in which one or multiple CPs (different scenarios) have been de-trended linearly or nonlinearly. The difference is estimated for Group 1 (linearly detrended) and Group 2 (nonlinearly detrended). Figure 6(a) represents the variations of ΔET_0, in which values of ET_0 were re-computed using linearly and nonlinearly detrended T_{max} (CP2). The total absolute ΔET_0 for CP2 is 3.19 mm d^{-1}, and that for nonlinear detrending is 0.6 mm d^{-1} (Table 5). Similarly, Figure 6(b,c) represents both sets of detrending considering CP3 (T_{min}) and CP4 (T_{max} and T_{min}) scenarios. Linear detrending ΔET_0 values of temperature factors are more substantial than those of nonlinear detrending ΔET_0, as shown in Table 5. In both the detrending methods, detrending T_{min} has the least influence on ET_0, followed by T_{max}'s detrending and combining the two temperature factors. Similarly, the linear and nonlinear detrending for scenarios (CP5–CP7) showed similar trends, i.e., the ΔET_0 values in both the cases are higher for scenarios CP6 and CP7 compared to scenario CP5 (Figure 6(d)–(f)). For linear detrending, the total absolute linear detrending differencing decreased from CP7 (3.47 mm d^{-1}) > CP6 (2.88 mm d^{-1}) > CP5 (0.77 mm d^{-1}) and for nonlinear detrending, total absolute linear detrending differencing decreased from CP6 (1.09 mm d^{-1}) > CP7 (0.99 mm d^{-1}) > CP5 (0.41 mm d^{-1}). The analysis also concludes that scenarios CP6 and CP7 have a similar influence on ET_0 on detrending; these will increase the value of ET_0 significantly for both the groups. In contrast, in the case of CP5, the average estimates of ΔET_0 move near to zero. Hence detrending RH_{max} has the least influence on ET_0. For the ΔET_0 variations of Group 1 and Group 2 for scenarios CP8 to

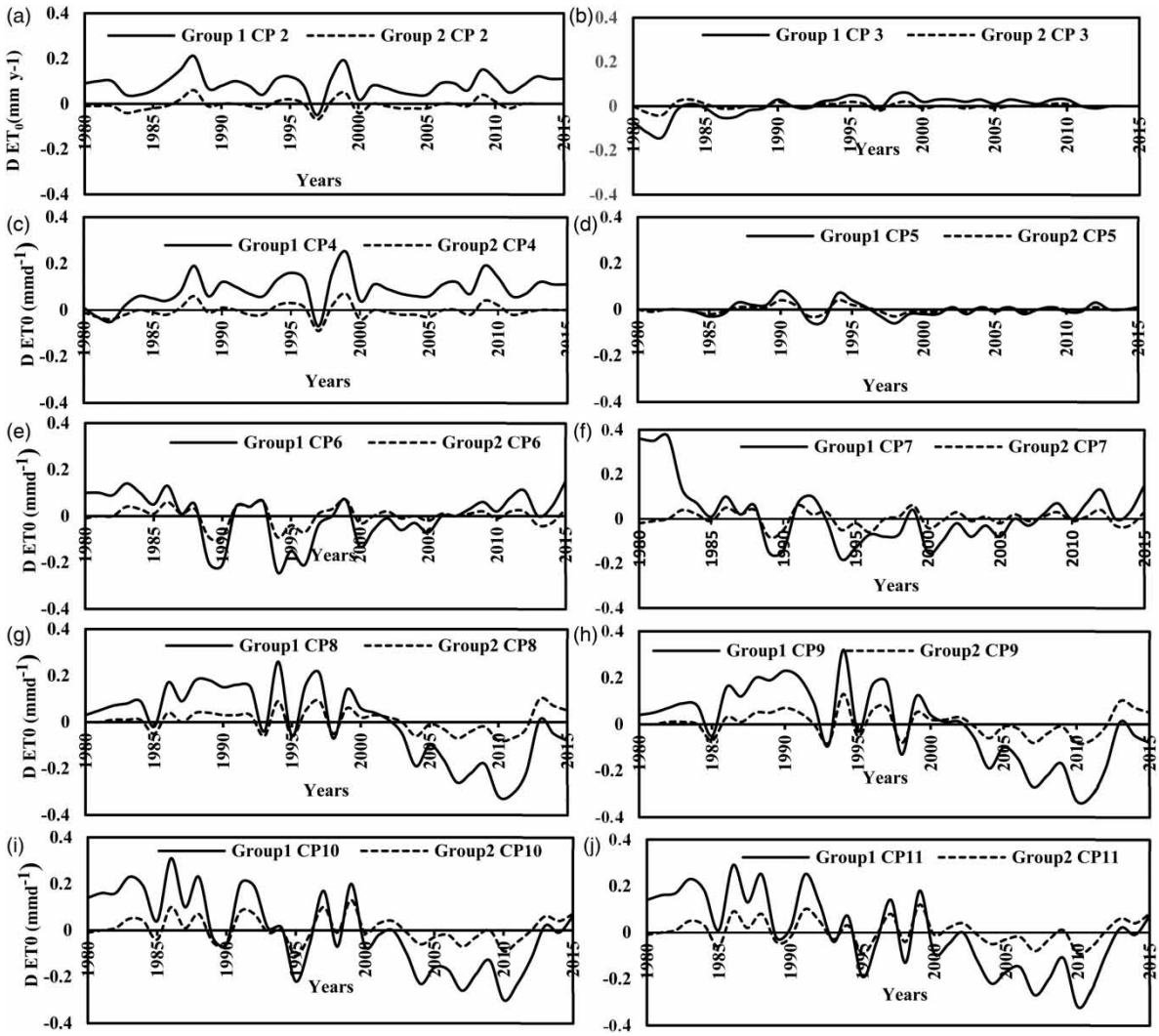

Figure 6 | ΔET_0 variation due to respective CPs for Group 1, and Group 2 over 1980–2015.

Table 5 | Statistical properties of ΔET_0 for CP2 to CP12 in Group 1 and Group 2

	Group 1				Group 2			
Scenarios	Maximum (mm d^{-1})	Minimum (mm d^{-1})	Abs. Sum (mm d^{-1})	Mean (mm d^{-1})	Maximum (mm d^{-1})	Minimum (mm d^{-1})	Abs. Sum (mm d^{-1})	Mean (mm d^{-1})
CP2	0.21	−0.05	3.19	0.09	0.06	−0.07	0.60	0.02
CP3	0.06	−0.14	1.07	0.03	0.03	−0.04	0.34	0.01
CP4	0.25	−0.07	3.37	0.09	0.07	−0.09	0.73	0.02
CP5	0.08	−0.06	0.77	0.02	0.04	−0.03	0.41	0.01
CP6	0.15	−0.24	2.88	0.08	0.07	−0.09	1.09	0.03
CP7	0.37	−0.18	3.47	0.10	0.06	−0.08	0.99	0.03
CP8	0.26	−0.32	4.62	0.13	0.10	−0.08	1.45	0.04
CP9	0.32	−0.33	4.80	0.13	0.13	−0.08	1.55	0.04
CP10	0.31	−0.30	4.85	0.13	0.13	−0.11	1.58	0.04
CP11	0.29	−0.32	4.90	0.14	0.12	−0.09	1.60	0.04
CP12	0.37	−0.24	4.12	0.11	0.18	−0.08	1.77	0.05

CP11, the pattern of detrending is the same, i.e., the ΔET_0 values for scenario CP8 and CP9, and CP10 and CP11 showed the same pattern, and similar to ΔET_0 values (Figure 6(g)–(j)). For linear detrending, total absolute linear detrending differencing decreased from CP11 (4.9 mm d^{-1}) > CP10 (4.85 mm d^{-1}) > CP9 (4.8 mm d^{-1}) > CP8 (4.62 mm d^{-1}). The same pattern was observed for nonlinear detrending, where total absolute differencing decreased from CP11 (1.6 mm d^{-1}) > CP10 (1.58 mm d^{-1}) > CP9 (1.55 mm d^{-1}) > CP8 (1.45 mm d^{-1}).

The value for absolute ΔET_0 is significantly higher for linear detrending than nonlinear detrending in all the cases. Hence, the influence of linear detrending is more significant than that of nonlinear detrending. From the analysis, it may be concluded that T_{min} (CP3) and RH_{max} (CP5) have the least influence on ET_0, whereas the most influencing independent climatic parameter was Sunshine duration (CP8).

ΔET_0 variations of Group 1 and Group 2 for scenario CP12

In both the linear and nonlinear detrending, the detrending pattern is the same for scenario CP12 (Figure 7). The maximum and minimum value of ΔET_0 for linear detrending was observed as 0.37 and −0.24 mm d^{-1} in 1988 and 2011. In nonlinear detrending, 0.18 mm d^{-1} was the maximum ΔET_0 in 1999, and −0.08 mm d^{-1} was the minimum value observed in the years 2004 and 2011. Total absolute linear detrending differencing for both linear and nonlinear detrending is 4.12 and 1.77 mm d^{-1}, respectively (Table 5).

Different statistical properties of ΔET_0 like maximum, minimum, and average ΔET_0 are represented in Figure 8. The ΔET_0 statistic for Group 1 is significantly higher than Group 2, which may be because meteorological data follow a nonlinear pattern. Hence, nonlinear detrended ET_0 is closer to actual ET_0, which resulted in the lowest ΔET_0 values. Therefore, it may be proposed that nonlinear detrending gives closer results to the benchmark ET_0 values than linear detrending. In all the ΔET_0

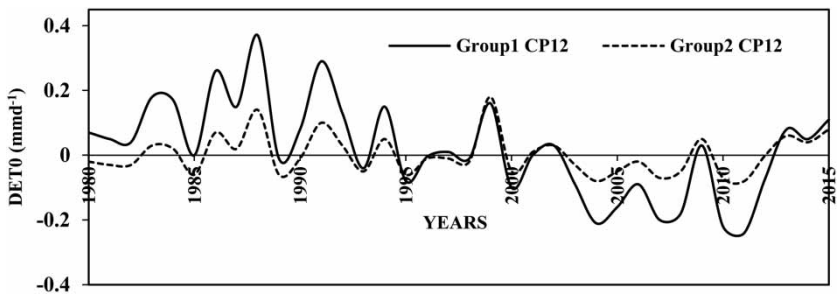

Figure 7 | ΔET_0 variation due to CP12 for Group 1, and Group 2 over 1980–2015.

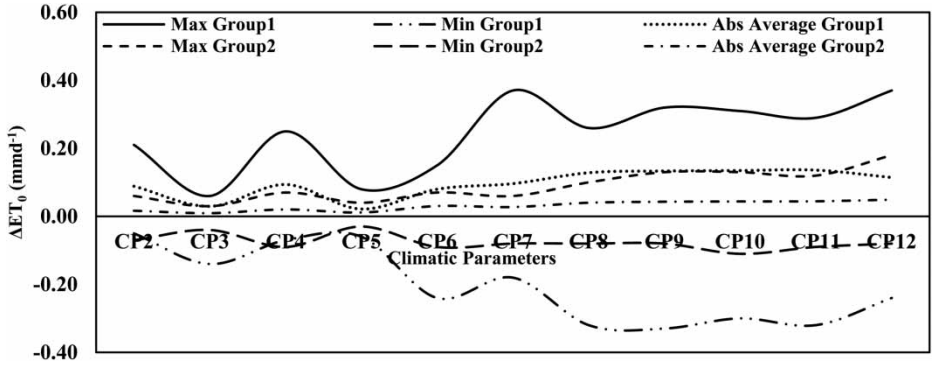

Figure 8 | Statistical properties of ΔET_0 for CP 2 to CP 12 in Group 1, and Group 2 over 1980 to 2015.

analyses, it is concluded that a significant difference was observed in all the CPs scenarios. For linear detrending, ΔET_0 values in all the cases are on the higher side. The similar values of ΔET_0 were found on the lower side in the case of nonlinear detrending.

DISCUSSION

Most CPs are stochastic and generally have non-normal distribution. Therefore, the application of linear detrending may be unable to capture trends correctly. Table 3 depicts the comparison between the linear RS (S) and Sen's slope (b) values of all the selected CPs, which helps to understand the similarity or differences between linear and nonlinear trending.

The results showed that the deviation between S and b values for CPs was small. Even though Sen's slope method is non-parametric and the linear RS method a parametric technique, the two approaches are linear. In this way, the slight dissimilarities between S and b estimates would prompt a very close outcome for examining detrending impacts on ET_0 and affirmed the appropriateness of utilizing S values to detrend CPs.

The scenario 12 (CP12) is the only case that combines both temperature and non-temperature parameters mainly because simultaneously detrending the temperature parameters (T_{max} and T_{min}) on declining ET_0 were the biggest when contrasted with the effects of detrending of single parameters. Furthermore, the effects of detrending SSH on decreasing ET_0 were much more significant than the detrending of temperature, RH parameters in all three cases (i.e., RH_{max} and RH_{min}), which highlighted that sunshine duration (SSH) plays the most vital role in decreasing ET_0 in the eastern Himalayan region.

The decreasing trend in ET_0 identified in this study is concurrent with many studies in India and worldwide. Pandey *et al.* (2016) concluded that SSH is the main factor driving the ET_0 process in Northeast India. Poddar *et al.* (2018), in a study on the humid environment in the western Himalayan region of India, reported that solar radiation and temperature are the crucial factors to control ET_0. Jhajharia & Singh (2011) stated that the decrease in SSH has a positive relationship with the diurnal temperature range (DTR) and evaporation, leading to a reduction in evapotranspiration in Northeast India. Goroshi *et al.* (2017), in a study of evapotranspiration over India, also reported a decreasing trend in ET_0 over northeast India. Patle *et al.* (2019), using sensitivity analysis for Gangtok, East Sikkim, concluded that ET_0 changes positively related to SSH and T factors. According to Li *et al.* (2014), one of the main reasons behind the decreasing trend of ET_0 in northwestern China is a decrease in DTR. All these studies generally agree that the SSH is the most influential parameter in modeling the evapotranspiration process, especially in the humid climate. The conclusion of our study of the original and re-estimated ET_0 found in both cases (linear and nonlinear detrended) CPs also similar to the studies mentioned above.

By relating the influence of eliminating trends (linear and nonlinear) from the CPs on ET_0 in Sikkim, dissimilarities were found for the recalculated ET_0 between Group 1 and Group 2 scenarios. Due to the seasonal periodicity in the CPs, including ET_0, the results from Group 2 were even more conclusive for assessing the impacts of global warming and climate change on ET_0.

The decrease of ET_0 results in reduced crop water/ irrigation requirements for crops and plants in the region. Diminished ET_0 would bring about increased overland flow. Accordingly, it may increase the flood risk due to accelerated snowmelt on the alpine zone in the summer season, resulted from increased temperature. Therefore, the region's wetter conditions under the present global warming scenarios and drier are subsequently detrending the CPs and re-evaluating dry spell conditions.

CONCLUSIONS

This study aims to identify the impacts of eliminating trends (linear and nonlinear) from the meteorological parameters (CPs) that drive ET_0 processes. Accordingly, 23 scenarios, including the non-de-trended ET_0 (CP1), and Group 1 (by eliminating linear trend from CPs) and Group 2 (by eliminating nonlinear pattern from CPs), were set to know how the CPs influenced ET_0 for the period 1980–2015 in Gangtok, East Sikkim. To study the influence of trend, the ET_0 was re-estimated after detrending the respective CPs and then compared with non-de-trended ET_0 (CP1). The main conclusions derived are as follows:

1. The difference between ET_0 and the detrended ET_0 (ΔET_0) was significantly higher for linear detrending (Group 1) as compared to nonlinear detrending (Group 2). For linear detrending, the maximum difference ΔET_0 was observed as 0.37 mm $d^{-1}$for CP 7 and CP 12 scenario, and the minimum difference was observed as -0.05 mm d^{-1} for CP 2.
2. In both the groups, the consistent mean difference of ΔET_0 was observed for CP 8 to CP 12 when sunshine duration and RH parameters were detrended. However, results from Group 2 were reasonable and conclusive as the Group 2 results were closer to those of the ET_0. The nonlinear detrending gives closer results to the original as compared to linear detrending.
3. The SSH was the most crucial parameter affected because there was the highest increase in ET_0 when SSH was detrended either in Group 1 linearly or nonlinearly in Group 2. A decline in SSH and T_{max} caused a general reduction of ET_0, which neutralized increased T_{min} and RH on ET_0.
4. The declines of T_{max} and increment of RH likewise added to the low abatement of ET_0. Overall, the combined impacts of all CPs caused the general decline of ET_0.
5. Additionally, the comparison of removing trends nonlinearly from single or multiple CPs may be useful to understand the changing pattern of ET_0 under global warming conditions.

AUTHOR'S CONTRIBUTION STATEMENT

Vanita Pandey studied the conception and design, acquisition of data and drafted the manuscript. **Indira Taloh** analysed and interpreted the data. **P. K. Pandey** edited and made critical revisions. All authors of this paper have directly participated in the writing, editing, planning, execution, and analysis of this study.

CONFLICT OF INTEREST

The authors declare that they have no known competing financial interests or personal relationships that could have appeared to influence the work reported in this paper.

DATA AVAILABILITY STATEMENT

Data cannot be made publicly available; readers should contact the corresponding author for details.

REFERENCES

Adarsh, S. & Janga Reddy, M. 2015 Trend analysis of rainfall in four meteorological subdivisions of southern India using nonparametric methods and discrete wavelet transform. *International Journal of Climatology* **35**, 1107–1124.

Aksu, H., Kuşçu, S. & Şimşek, O. 2010 *Trend Analysis of Hydrometeorological Parameters in Climate Regions of Turkey*. Journal BALWOIS2010, Ohrid, Republic of Macedonia.

Allen, R. G., Perevia, L. S., Raes, D. & Smith, M. 1998 *Crop Evapotranspiration: Guidelines for Computing Crop Water Requirements*. FAO Irrigation and Drainage Paper No. 56. Food and Agriculture Organization, Rome, Italy.

Antico, A., Schlotthauer, G. & Torres, M. E. 2014 Analysis of hydroclimatic variability and trends using a novel empirical mode decomposition: application to the Paraná River Basin. *Journal of Geophysical Research: Atmospheres* **119**, 1218–1233.

Azizzadeh, M. & Javan, K. 2015 Analyzing trends in reference evapotranspiration in Northwest part of Iran. *Ecological Engineering* **16**, 1–12.

Burn, D. H. & Hesch, N. M. 2007 Trends in evaporation for Canadian Prairies. *Journal of Hydrology* **336**, 61–73.

Dinpashoh, Y., Jhajharia, D., Fakheri-fard, A., Singh, V. P. & Kahya, E. 2011 Trends in reference crop evapotranspiration over Iran. *Journal of Hydrology* **399** (3), 422–433.

Donohue, R. J., McVicar, T. R. & Roderick, M. L. 2010 Assessing the ability of potential evaporation formulations to capture the dynamics in evaporative demand within a changing climate. *Journal of Hydrology* **386**, 186–197.

Espadafor, M., Lorite, I. J., Gavilán, P. & Berengena, J. 2011 An analysis of the tendency of reference evapotranspiration estimates and other climate variables during the last 45 years in Southern Spain. *Agricultural Water Management* **98** (6), 1045–1061.

Ghafouri-Azar, M., Bae, D.-H. & Kang, S. U. 2018 Trend analysis of long-term reference evapotranspiration and its components over the Korean Peninsula. *Water* **10**, 1373.

Gocic, M. & Trajkovic, S. 2014 Analysis of trends in reference evapotranspiration data in a humid climate. *Hydrological Sciences Journal* **59** (1), 165–180.

Golubev, V. S., Lawrimore, J. H., Groisman, P. Y., Speranskaya, N. A., Zhuravin, S. A., Menne, M. J., Peterson, T. C. & Malone, R. W. 2001 Evaporation changes over the contiguous United States and the former USSR: a reassessment. *Geophysical Research Letters* **28**, 2665–2668.

Goroshi, S., Pradhan, R., Singh, R. P., Singh, K. K. & Parihar, S. J. 2017 Trend analysis of evapotranspiration over India: observed from long-term satellite measurement. *Journal of Earth System Science* **126**, 113.

Government of India 1989 *Agroclimatic Regional Planning. An Overview, Planning Commission, New Delhi*. Government Printing Press, New Delhi, India.

Guo, B., Chen, Z., Guo, J., Liu, F., Chen, C. & Liu, K. 2016 Analysis of the nonlinear trends and non-stationary oscillations of regional precipitation in Xinjiang, Northwestern China, using ensemble empirical mode decomposition. *International Journal of Environmental Research and Public Health* **13**, 345.

Hameed, K. H. & Rao, A. R. 1998 A modified Mann-Kendall trend test for autocorrelated data. *Journal of Hydrology* **204** (1–4), 182–196.

Huang, N. E., Shen, Z., Long, S. R., Wu, M. C., Shih, S. H., Zheng, Q., Tung, C. C. & Liu, H. H. 1998 The empirical mode decomposition method and the Hilbert spectrum for non-stationary time series analysis. *Proceedings of the Royal Society of London. Series A* **454**, 903–995.

Huo, Z., Dai, X., Feng, S., Kang, S. & Huang, G. 2013 Effect of climate change on reference evapotranspiration and aridity index in arid region of China. *Journal of Hydrology* **492**, 24–34.

IPCC 2019 *Climate Change and Land: An IPCC Special Report on Climate Change, Desertification, Land Degradation, Sustainable Land Management, Food Security, and Greenhouse gas Fluxes in Terrestrial Ecosystems* (Shukla, P. R., Skea, J., Calvo Buendia, E., Masson-Delmotte, V., Pörtner, H.-O., Roberts, D. C., Zhai, P., Slade, R., Connors, S., van Diemen, R., Ferrat, M., Haughey, E., Luz, S., Neogi, S., Pathak, M., Petzold, J., Portugal Pereira, J., Vyas, P., Huntley, E., Kissick, K., Belkacemi, M. & Malley, J., eds). IPCC, Geneva, Switzerland.

Jayawardene, H. K. W. I., Sonnadara, D. U. J. & Jayewardene, D. R. 2005 Trends of rainfall in Sri Lanka over the last century. *Sri Lankan Journal of Physics* **6**, 7–17.

Jhajharia, D. & Singh, V. P. 2011 Trends in temperature, diurnal temperature range and sunshine duration in Northeast India. *International Journal of Climatology* **31**, 1353–1367.

Jhajharia, D., Dinpashoh, Y., Kahya, E., Singh, V. P. & Fakheri-Fard, A. 2012 Trends in reference evapotranspiration in the humid region of northeast India. *Hydrological Processes* **26**, 421–435.

Jones, J. R., Schwartz, J. S., Ellis, K. N., Hathaway, J. M. & Jawdy, C. M. 2015 Temporal variability of precipitation in the Upper Tennessee Valley. *Journal of Hydrology: Regional Studies* **3**, 125–138.

Kahya, E. & Kalayci, S. 2004 Trend analysis of streamflow in Turkey. *Journal of Hydrology* **289**, 128–144.

Karmeshu, N. 2012 Trend detection in annual temperature & precipitation using the Mann Kendall test – a case study to assess climate change on select states in the northeastern United States. *Master of Environmental Studies Capstone Projects* **47**, 1–33.

Kendall, M. G. 1975 *Rank Correlation Methods*, 4th eds. Charles Griffin, London.

Kousari, M. R. & Ahani, H. 2012 An investigation on reference crop evapotranspiration trend from 1975 to 2005 in Iran. *International Journal of Climatology* **32**, 2387–2402.

Li, L., Chi, D. C. & Zhang, Z. L. 2007 Analysis of the change characteristics and effect factors of reference evapotranspiration in Taizi river basin. *Transactions of the CSAE* **23**, 34–38.

Li, X., Liang, S., Yuan, W., Yu, G., Cheng, X., Chen, Y., Zhao, T., Feng, J., Ma, Z., Ma, M., Liu, S., Chen, J., Shao, C., Li, S., Zhang, X., Zhang, Z., Sun, G., Chen, S., Ohta, T., Varlagin, A., Miyata, A., Takagi, K., Saiqusa, N. & Kato, T. 2014 Estimation of evapotranspiration over the terrestrial ecosystems in China. *Ecohydrology* **7** (1), 139–149.

Li, Y., Yao, N. & Chau, H. 2017 Influences of removing linear and nonlinear trends from climatic variables on temporal variations of annual reference crop evapotranspiration in Xinjiang, China. *Science of The Total Environment* **592**, 680–692.

Liu, Q., Yang, Z. & Cui, B. 2008 Spatial and temporal variability of annual precipitation during 1961–2006 in Yellow River Basin, China. *Journal of Hydrology* **361**, 330–338.

Liu, W., Zhang, B. & Han, S. 2020 Quantitative analysis of the impact of meteorological factors on reference evapotranspiration Changes in Beijing, 1958–2017. *Water* **12**, 2263.

Luukko, P. J. J., Helske, J. & Räsänen, E. 2016 Introducing Rlibeemd: a program package for performing the ensemble empirical mode decomposition. *Computational Statistics* **31**, 545–557.

Mann, H. B. 1945 Nonparametric tests against trend. *Econometrica* **33**, 245–259.

Marusiak, O. & Pekar, J. 2014 Analysis of multiannual fluctuations and long-term hydrological time series trends. In: *Proceedings of Advances in Environmental Science – Development and Chemistry*, 17–21 July 2014, Greece, pp. 156–159.

McKenney, M. S. & Rosenberg, N. J. 1993 Sensitivity of some potential evapotranspiration estimation methods to climate change. *Agricultural and Forest Meteorology* **64** (1), 81–110.

McVicar, T. R., Roderick, M. L., Donohue, R. J., Li, L. T., VanNiel, T. G., Thomas, A., Grieser, J., Jhajharia, D., Himri, Y., Mahowald, N. M., Mescherskaya, A. V., Kruger, A. C., Rehman, S. & Dinpashoh, Y. 2012 Global review and synthesis of trends in observed terrestrial near-surface wind speeds: implications for evaporation. *Journal of Hydrology* **416–417**, 182–205.

Mo, X., Chen, X., Hu, S., Liu, S. & Xia, J. 2017 Attributing regional trends of evapotranspiration and gross primary productivity with remote sensing: a case study in the North China Plain. *Hydrology and Earth System Sciences* **21**, 1–32.

Niu, Z., Honglin, H., Gaofeng, Z., Ren, X., Zhang, L., Zhang, K., Yu, G., Ge, R., Li, P., Zeng, N. & Zhu, X. 2019 An increasing trend in the ratio of transpiration to total terrestrial evapotranspiration in China from 1982 to 2015 caused by greening and warming. *Agricultural and Forest Meteorology* **279**, 107701.

Pandey, P. K., Dabral, P. P. & Pandey, V. 2016 Evaluation of reference evapotranspiration methods for the northeastern region of India. *International Soil and Water Conservation Research* **4** (1), 52–63.

Patle, G. & Singh, D. K. 2015 Sensitivity of annual and seasonal reference crop evapotranspiration to principal climatic variables. *Journal of Earth System Science* **124** (4), 819–829.

Patle, G. T., Sengdo, D. & Tapak, M. 2019 Trends in major climatic parameters and sensitivity of evapotranspiration to climatic parameters in the eastern Himalayan region of Sikkim, India. *Journal of Water and Climate Change* jwc2019121. https://doi.org/10.2166/wcc.2019.121.

Poddar, A., Gupta, P., Kumar, N., Shankar, V. & Ojha, C. S. P. 2018 Evaluation of reference evapotranspiration methods and sensitivity analysis of climatic parameters for sub-humid sub-tropical locations in western Himalayas (India). *ISH Journal of Hydraulic Engineering* 1–11.

Salas, J. D., Delleur, J. W., Yevjevich, V. & Lane, W. L. 1980 *Applied Modeling of Hydrologic Time Series*. Water Resources Publications Ltd., Littleton, CO, p 484.

Sang, Y. F., Wang, Z. & Liu, C. 2014 Comparison of the MK test and EMD method for trend identification in hydrological time series. *Journal of Hydrology* **510**, 293–298.

Sayemuzzaman, M. & Jha, M. K. 2014 Seasonal and annual precipitation time series trend analysis in North Carolina, United States. *Atmospheric Research* **137**, 183–194.

Sen, P. K. 1968 Estimates of the regression coefficient based on Kendall's tau. *Journal of the American statistical association* **63**, 1379–1389.

Shadmani, M., Marofi, S. & Roknian, M. 2012 Trend analysis in reference evapotranspiration using Mann-Kendall and Spearman's Rho Tests in Arid Regions of Iran. *Water Resource Management* **26**, 211–224.

Sonali, P. & Nagesh Kumar, D. 2013 Review of trend detection methods and their application to detect temperature changes in India. *Journal of Hydrology* **476**, 212–227.

Sonali, P. & Nagesh Kumar, D. 2016 Spatio-temporal variability of temperature and potential evapotranspiration over India. *Journal of Water and Climate Change* **7** (4), 810–822.

Tabari, H. & Marofi, S. 2011 Changes of Pan Evaporation in the West of Iran. *Water Resources Management* **25**, 97–111.

Tabari, H. & Hosseinzadeh Talaee, P. 2014 Sensitivity of evapotranspiration to climatic change in different climates. *Global and Planetary Change* **115**, 16–23.

Thepprasit, C., Pongput, K. & Supriyasilp, T. 2009 Reference evapotranspiration trend analysis in the upper Chao Phraya river basin. *Thai Journal of Agricultural Science* **42** (4), 201–211.

Torres, M. E., Colominas, M. A., Schlotthauer, G. & Flandrin, P. 2011 A Complete ensemble empirical mode decomposition with adaptive noise. In: *IEEE International Conference on Acoustics, Speech and Signal Processing (ICASSP),* May 22–27, 2011, Prague, Czech Republic, pp. 4144–4147.

Verma, I. J., Jadhav, V. N. & Erande, R. S. 2008 Recent variations and trends in potential evapotranspiration (PET) over India. *MAUSAM* **59** (1), 119–128.

Xu, C., Gong, L., Jiang, T., Chen, D. & Singh, V. 2006 Analysis of spatial distribution and temporal trend of reference evapotranspiration and pan evaporation in Changjiang (Yangtze River) catchment. *Journal of Hydrology* **327** (1), 81–93.

Yadav, S., Deb, P., Kumar, S., Pandey, V. & Pandey, P. 2016 Trends in major and minor meteorological variables and their influence on reference evapotranspiration for mid Himalayan region at east Sikkim, India. *Journal of Mountain Sciences* **13**, 302–315.

Yue, S., Pilon, P., Phinney, B. & Cavadias, G. 2002 The influence of autocorrelation on the ability to detect trend in hydrological series. *Hydrological Processes* **16**, 1807–1829.

Yue, S., Pilon, P. & Phinney, B. 2003 Canadian streamflow trend detection: impacts of serial and cross-correlation. *Hydrological Science Journal* **48** (1), 51–63.

Yue, S. & Wang, C. 2004 The Mann-Kendall test modified by effective sample size to detect trend in serially correlated hydrological series. *Water Resource Management* **18** (3), 201–218.

Zaninović, K. & Gajić-Čapka, M. 2000 Changes in components of the water balance in the Croatian Lowlands. *Theoretical and Applied Climatology* **65**, 111–117.

Zhao, L., Xia, J., Sobkowiak, L. & Li, Z. 2014 Climatic characteristics of reference evapotranspiration in the Hai river basin and their attribution. *Water* **6**, 1482–1499.

First received 2 June 2020; accepted in revised form 12 May 2021. Available online 12 June 2021